Smart Structures and Systems, Vol. 2, No. 1 (2006) 61-80 61
DOI: http://dx.doi.org/10.12989/sss.2006.2.1.061

Vibration control of mechanical systems using semi-active MR-damper

Dipak K. Maiti†

Department of Aerospace Engineering, Indian Institute of Technology, Kharagpur-721302, India

P. P. Shyju‡

Department of Civil Engineering, Malnad College of Engineering, Hassan, India

K. Vijayaraju‡†

Airframe Directorate, Aeronautical Development Agency, Vimanapura, Bangalore-560017, India

(Received August 1, 2005, Accepted December 23, 2005)

Abstract. The concept of structural vibration control is to absorb vibration energy of the structure by introducing auxiliary devices. Various types of structural vibration control theories and devices have been recently developed and introduced into mechanical systems. One of such devices is damper employing controllable fluids such as ElectroRheological (ER) or MagnetoRheological (MR) fluids. MagnetoRheological (MR) materials are suspensions of fine magnetizable ferromagnetic particles in a non-magnetic medium exhibiting controllable rheological behaviour in the presence of an applied magnetic field. This paper presents the modelling of an MR-fluid damper. The damper model is developed based on Newtonian shear flow and Bingham plastic shear flow models. The geometric parameters are varied to get the optimised damper characteristics. The numerical analysis is carried out to estimate the damping coefficient and damping force. The analytical results are compared with the experimental results. The results confirm that MR damper is one of the most promising new semi-active devices for structural vibration control.

Keywords: MagnetoRheological fluid; MR damper; Bingham plastic model; Newtonian fluid; vibration; nose landing gear.

1. Introduction

The consequences of vibrations of a mechanical system are usually undesirable and are often important design considerations. Structural vibration control techniques are believed to be one of the promising routes for avoiding the ill effects of vibrations. The aim of structural vibration control is to absorb vibration energy of the structure by introducing auxiliary devices. Various types of structural

†Assistant Professor, Corresponding Author, E-mail: dkmaiti@aero.iitkgp.ernet.in
‡M. E. Student, E-mail: shyjupp@yahoo.com
‡†DPD(Composite & Smart Materials), E-mail: vijay@jetmail.ada.gov.in

vibration control theories and devices have recently been developed and introduced into mechanical systems. One of such devices is damper employing controllable fluids such as ElectroRheological (ER) or MagnetoRheological (MR) fluids. MagnetoRheological (MR) materials are suspensions of fine magnetizable ferromagnetic particles in a non-magnetic medium exhibiting controllable rheological behaviour in the presence of an applied magnetic field. The MR fluid, which is a counterpart of ER material, is the most widely used fluid among the controllable rheological materials. A typical MR fluid consisted of 9 parts by weight of carbonyl iron to one part of silicone oil, petroleum oil or kerosene (David 2001, Dyke, *et al*. 1996). They studied the static and dynamic properties of chain formation in MR fluids. Their work focused on the initial stage "Magneto-Rehological Fluids" of the structural transition. Later MR fluid was synthesised and marketed by Lord Corporation (Jolly, *et al*. 1998).

The MR fluids are becoming increasingly important in various applications concerning semi-active vibration control or torque transfer. Shock absorbers (Lord Material Division) and vibration dampers (Kelso 2001) are the most exciting applications of MR fluid. Gravatt (2003) developed a semi-actively damped super-sport motorcycle system using MR fluids. He retrofitted the MR damper in the front suspension with control system for the super-sport motorcycle. Simon (1998) evaluated experimentally the performance of semi-active MagnetoRheological primary suspension on a heavy truck. The commercial applications of MR dampers include heavy-duty vehicle seat suspensions, rotary brakes that provide tuneable resistance for exercise equipment, vibration dampers for washing machines (Lord Material Division 1999) as well as prosthetic devices and MR pneumatic actuators (Lord Material Division 1999) using MR technology (MR fluid dampers). Kang (2001) investigated the helicopter blade lag damping using embedded chordwise absorbers. Kruger, *et al*. (2000) developed a feedback control system for the MR damper adapted in the semi-active landing gear for transport aircraft using fuzzy controller and skyhook controller.

This paper presents the modelling and design of an MR-fluid damper primarily consisting of a cylinder and a piston rod. The MR fluid flows through the annular gap between piston and the sidewalls of the cylinder when piston moves with velocity. The copper wires are wound around the piston in three spools to generate magnetic field. The damper model is developed based on Newtonian shear flow and Bingham plastic shear flow models. The geometric parameters are varied to get the optimised damper characteristics. The numerical analysis is carried out to estimate the damping coefficient and damping force. Then the dynamic behaviour of the damper is simulated based on the programme developed using MATLAB. The designed damper model is fabricated and tested to characterise the damper. The experimental results are compared with the analytical results. These studies establish that an MR damper is one of the most promising semi-active devices for structural vibration control.

2. MR fluid

Magneto-rheological fluids exhibit a change in rheological properties when a magnetic field is induced through the fluid. In essence, one of the important fluid flow characteristics, namely apparent viscosity, changes with the intensity of magnetic field. MR fluids are quite similar to ER fluids and Ferro-fluids in composition: all three fluids are a non-colloidal suspension of polarizable particles (Lord Material Division, "Magneto-Rehological Fluids"). While MR and ER fluids usually contain carbonyl iron of the order of a few microns in size (Jolly, *et al*. 1998), ferrofluids use nanometer-sized iron-oxide particles. MR fluid is highly preferred to other fluids due to its inherent property of having very high yield strength. It is worth to mention here that the Ferrofluid particles are too small to demonstrate any

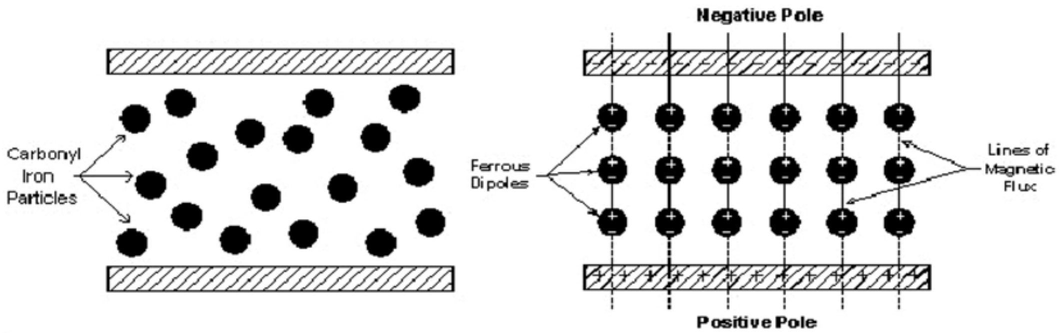

Fig. 1 Off state MR fluid particles (Left) and aligning in an applied magnetic field (Right)

yield strength and the yield strength of ER fluid ranges only from 0.02 to 0.05 times the strength of MR fluid (Lord Material Division, "Magneto-Rehological Fluids").

In the absence of magnetic field (off state), MR fluids behave like any other Newtonian fluid (Lord 1999). Application of an external magnetic field through MR fluid containing micron sized particles results in the formation of magnetic dipoles. The dipoles align parallel to the induced magnetic flux lines to form chain-like structures of iron particles between the North and South poles (Kang 2001) as shown in Fig. 1.

The ferrous particles that form each of the chains resist movement of fluid in a direction normal to that of the flux lines, and the amount of resistance is proportional to the intensity of the applied magnetic field.

2.1. Bingham flow model

Bingham fluid is characterised by a sort of yield stress below which the fluid does not flow, while above it, it begins to flow with a constant viscosity as if it is a Newtonian fluid (Lord Material Division, "Magneto-Rehological Fluids"). The Newtonian and an idealised Bingham plastic model are shown in Fig. 2.

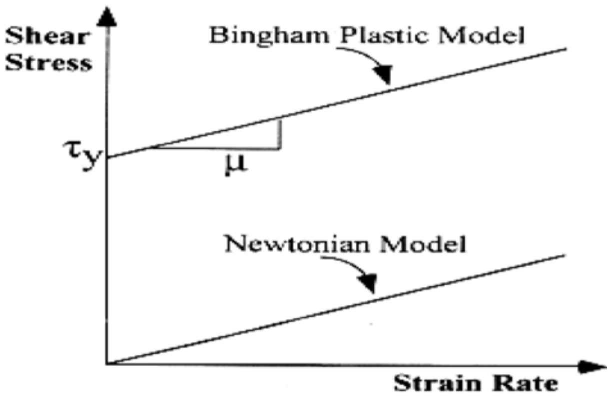

Fig. 2 The idealised Bingham plastic model and the Newtonian model

The Bingham fluid (Fig. 2) can be modelled as given by

$$\tau = \tau_y + \mu\,\dot{\gamma} \qquad (\text{for } \tau > \tau_y) \tag{1}$$

In Eq. (1) τ_y is the limiting shear stress beyond which the fluid flows with a constant viscosity μ. The value of τ_y is zero for the case of a Newtonian fluid.

3. Mathematical model

3.1 Design of MR damper

The schematic diagram and the cross sectional details of the MR damper are shown in Fig. 3. The variables, which are considered in the design, are classified into two types, namely controllable variables and uncontrollable variables. The controllable variables are those which could be varied during the use of the system. They are mainly the magnetic field, electric current, etc. At the end of the design, geometric and constructional parameters are finalized. Hence these latter parameters are called uncontrollable variables. These include geometric parameters and coil position and dimensions. Various design parameters marked on the schematic diagram are described as L_p - pole length, t_w - cylinder wall thickness, t_g - annular gap, D_c - diameter of core, D_b - inner diameter of cylinder and D_r - Diameter of piston rod.

In the geometric design, initial iterations were carried out varying the magnetic field and the annular gap while the other geometric parameters are kept unchanged. This was carried out to establish the relationship between the force developed as the magnetic field increases and also the effect of varying annular gap on the damping coefficient. The computations are carried out with a program developed in MATLAB based on the mathematical formulation reported in Gavin, *et al.* (2001).

MR dampers generally use either the pressure driven the flow (valve) mode or direct-shear mode of the fluid. There are two independent sets of equations used to determine the MR damper force in the different modes. Pressure driven flow mode has two components to the pressure drop: pressure loss due to viscous drag, and pressure loss due to the field dependent yield stress, as shown in Eq. (2).

$$\Delta P = \Delta P_\eta + \Delta P_\tau = \frac{12\,\eta Q L}{t_g^3 w} + \frac{c\,\tau_y L}{t_g} \tag{2}$$

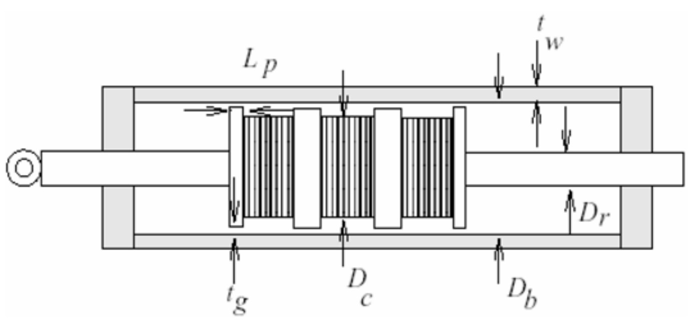

Fig. 3 Cross section of MR damper

where, ΔP is the total pressure drop, ΔP_η is the viscous pressure loss, ΔP_τ is the field dependent yield stress pressure loss, η is the fluid viscosity, Q is the flow rate that depends on the piston velocity (V_p), L is the total pole length, w is the pole width, t_g is the fluid gap, and τ_y is the field dependent yield stress. The variable c ranges from a minimum value of 2 (for $\Delta P_\tau/\Delta P_\eta < 1$) to a maximum value of 3 (for $\Delta P_\tau/\Delta P_\eta > 100$). The damping force of a direct-shear device is based on the shear stress developed along the piston surface due to a combination of the viscous effects of the fluid and the field induced yield stress (Lord 1999). The force F generated in the device can be expressed as the pressure drop times the piston cross sectional area given as

$$F = \Delta P \frac{\pi}{4}((D_p + 2t_g)^2 - D_r^2) \tag{3}$$

The viscous damping constant can also be expressed as

$$F_\eta = CV_p \tag{4}$$

where the damping coefficient C is function of geometric and magnetic circuit parameters.

3.2. Magnetic circuit design

After fixing all the parameters described above, it is required to design the magnetic circuit capable of generating a maximum flux of 0.6 Tesla. The task is to design a magnetic circuit (the path of the magnetic flux) and to estimate the required amp-turns (NI). An optimal design of the magnetic circuit requires maximising magnetic field energy in the fluid gap and minimising the loss of energy in steel flux conduit and in the regions of non-working areas (Lord 1999). The total quantity of steel in the magnetic circuit also needs to be minimised. However the cross-sectional area of steel should be such that the field intensity is low. The MR damper magnetic circuit typically uses low carbon steel, which has a high magnetic permeability and saturation, as a magnetic flux conduit to guide and focus magnetic flux into the fluid gap.

It is to be mentioned here that some minor factors like, non-linear magnetic properties of MR fluid and steel, possible losses at junctions and boundaries, limits on voltage, current, inductance, possible inclusion of permanent magnets for fail-safe operation, and eddy currents have not been considered in the present design.

The typical design process for magnetic circuit (Lord 1999) is as follows:

(i) Determine the magnetic field intensity H_f in the MR fluid from the B-H curve of the MR fluid in Fig. 4.

(ii) The total magnetic induction flux is given by

$$\Phi = B_f A_f \tag{5}$$

where A_f is the effective pole area including the fringe of magnetic flux.

(iv) Using the principle of continuity of magnetic flux, determine the magnetic induction B_s in the steel. Continuity of magnetic flux is given by

$$\Phi = \Phi_{fluid} = \Phi_{steet} \tag{6}$$

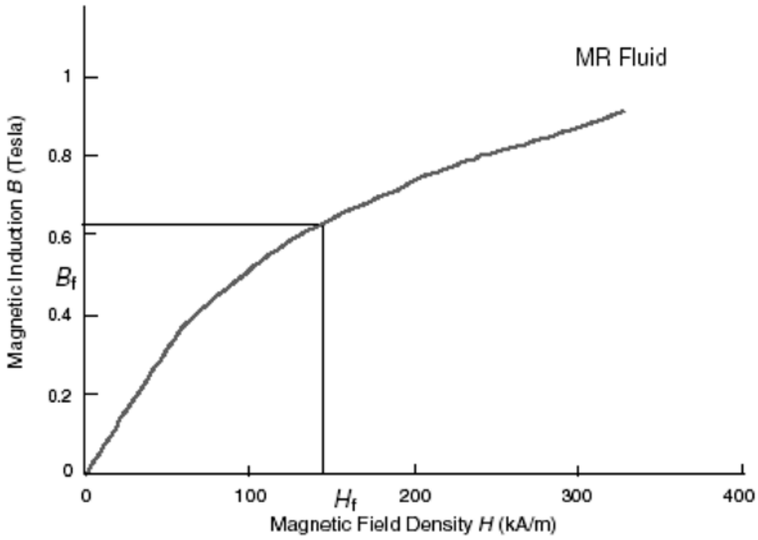

Fig. 4 B-H curve of MR fluid (Lord 1999)

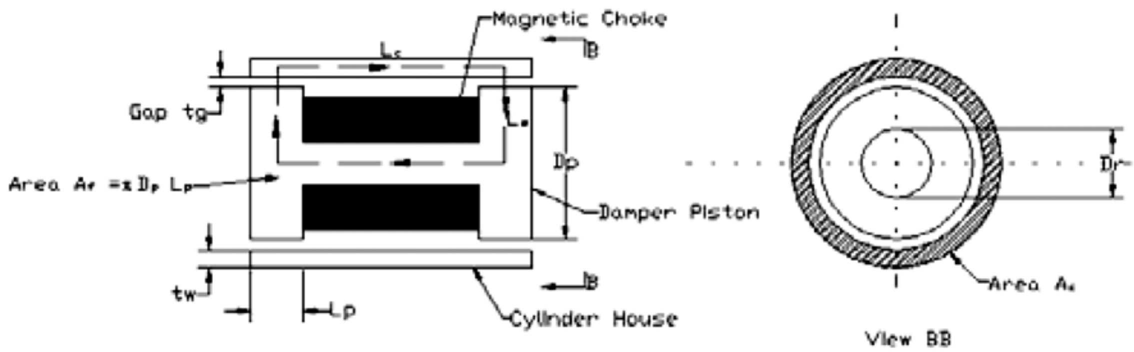

Fig. 5 One spool of piston rod to show the magnetic circuit of an MR damper

Then the magnetic induction in steel is given by

$$B_s = \frac{\Phi}{A_s} = \frac{B_f A_f}{A_s} \tag{7}$$

where A_s is area of section of cylinder steel (Fig. 5).

(v) Determine the magnetic field intensity H_s in the steel from the B-H curve (Fig. 6) of the steel.

(vi) Using the Kirchoffs's Law of magnetic circuits, the necessary number of amp-turns (NI) is

$$\mathrm{NI} = \Sigma H_i L_i = H_f g + H_s L \tag{8}$$

where g = total length of gaps (equal to 2 * t_g; Fig. 5), and L = length of steel path which is equal to L_s+L_c.

Most of the design parameters directly influence the behaviour of the magnetic circuit, and by choosing the parameters properly, MR devices with fast response times and low power requirements

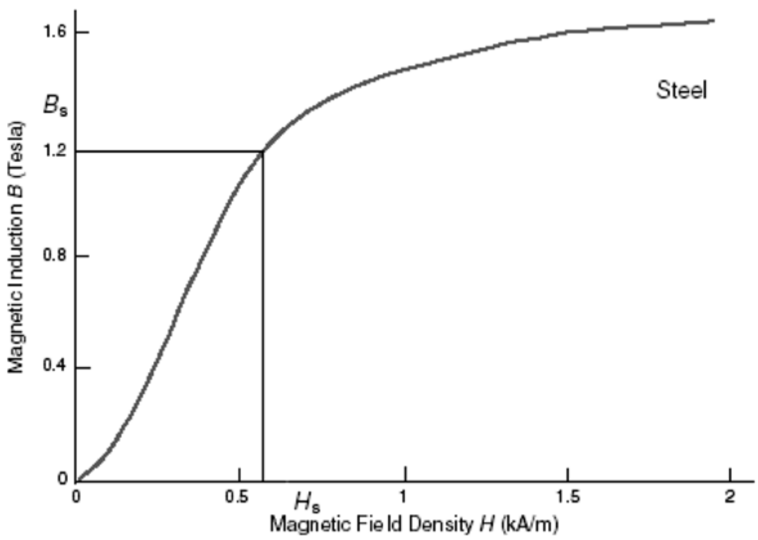

Fig. 6 B-H curve of the steel (Lord 1999)

can be designed. At high magnetic fields, magnetic materials become magnetically saturated.

To balance the power requirements of the device and the flux density in the MR material, it is advantageous to design the magnetic circuit in such a way that under operating conditions all of the components are below their saturation fields. An additional benefit of operating at lower flux densities is that the remnant magnetisation of the magnetic circuit and MR material is diminished.

3.3. Geometric design & fabrication

The design task is to choose an appropriate gap size t_g and active pole length L_p for a desired damping force. The design task is not straight forward, as this is a multi-parameter problem. Amongst the cylinders of standard diameter and thickness available in the market, a cylinder of internal diameter 40 mm and of wall thickness 4 mm is selected so as to satisfy the stability and strength criteria of the

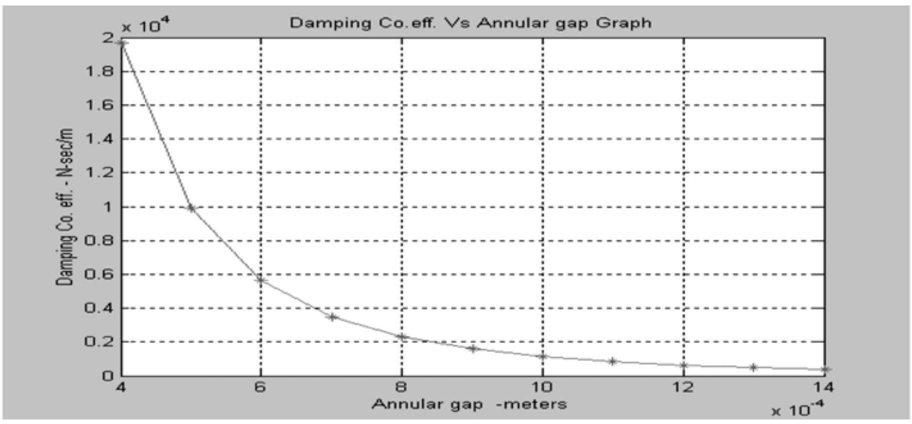

Fig. 7 Damping co-efficient vs annular gap

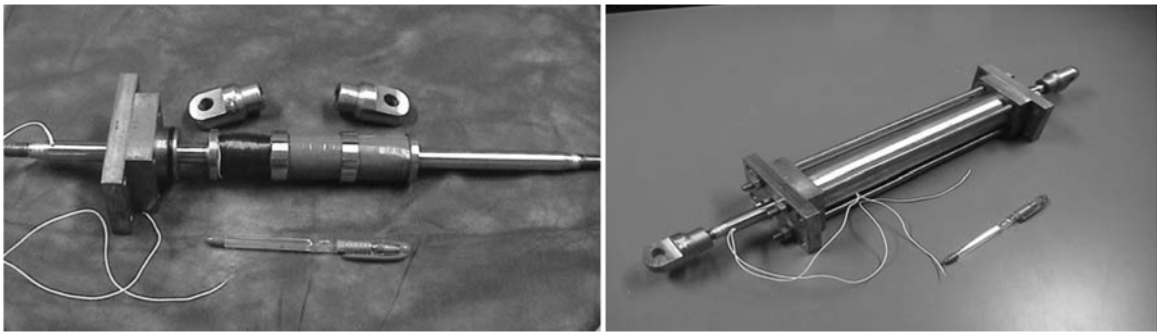

Fig. 8 Magnetic spools after winding & assembled MagnetoRheological damper

damper system. A 16 mm diameter (D_r) piston rod is used. For an annular gap of t_g, the piston head diameter (D_p) works out to be (40-2 t_g) mm. Three numbers of spools (N_s) are provided. The viscosity of the MR fluid used in the damper is 0.09 Pa-sec.

It is required to estimate the damping force offered by the damper with the application of varied magnetic field. One of the important parameter to establish this is the size of the annular gap. After fixing the above preliminary dimensions and using Eq. (3), the graph showing variation of damping coefficient with the size of the annular gap (t_g) has been drawn in Fig. 7 for 0.4 mm $< t_g <$ 1.4 mm. From the graph, it can be observed that the rate of change of damping co-efficient is quite high for small values of t_g. The value of damping coefficient is found to vary from 2×10^4 N-sec/m to 0.5×10^3 N-sec/m for $0.4 \leq t_g \leq 1.4$ mm. In order to give a longer life to the damper, which is generally subjected to cyclic loading during the course of its designed life, a gap of 1 mm is considered for fabrication. Based on the designed parameters the damper is fabricated. The fabricated damper is shown in Fig. 8.

4. Dynamic behaviour and simulation

One of the models commonly used to describe the behaviour of MR dampers is based on the properties of Bingham solids. The Bingham model of an MR fluid includes a variable rigid perfectly plastic element connected in parallel to a Newtonian viscous element, so that stress-strain constitutive relationship can be expressed as (see Fig. 2 and Eq. 1).

$$\begin{aligned} &\tau = \mu\,\dot{\gamma} + \tau_y(H)\,\mathrm{sgn}(\dot{\gamma}) \quad && \text{if } \tau > \tau_y \\ &\tau = G\gamma, \quad \dot{\gamma} = 0 && \text{if } \tau < \tau_y \end{aligned} \tag{9}$$

where, τ is the shear stress in the fluid, μ is the Newtonian viscosity independent of the applied magnetic field, $\dot{\gamma}$ is the shear strain rate, τ_y is the yielding shear stress controlled by the applied field H, and G is the shear modulus of the material. The fluid behaves viscoelastically until the shear stress approaches the critical value τ_y, whereas it moves like a Newtonian fluid as soon as such critical value is exceeded. The Bingham behaviour of an MR damper can then be derived from Eq. (9) through the study of an axisymmetric model of the flow. As a result, the force in the damper can approximately be expressed as

$$F_d = C_d\, U + F_{dy}\,(i)\,\mathrm{sgn}(U) \tag{10}$$

i.e., the sum of the two components, due to the fluid viscosity and due to the magnetic field-induced yield stress. U is the relative velocity of the piston with respect to the cylinder, C_d is the viscous damping constant and F_{dy} is the variable plastic threshold controlled by the applied magnetic field which, in turn depends on the current i in the coil inside the MR damper. Here varying the current in the coils from zero to a maximum value, it is possible to obtain a fairly wide range of plastic thresholds from a minimum value of $F_{\mathrm{dy,min}}$ due to the friction force of the bearing to a maximum value of $F_{\mathrm{dy,max}}$ due to the magnetic saturation. The effective force-displacement and force-velocity curves are generated based on the following numerical model as reported by Occhiuzzi, *et al*. (2003):

$$F_d = C_d\, U + [(F_{\mathrm{dy,max}} - F_{\mathrm{dy,min}})\; i\,/\,i_{\mathrm{max}}]\;\mathrm{sgn}(U) \tag{11}$$

5. Experimental setup

The fabricated MR Damper is tested in the laboratory by using a servo-hydraulic actuator controlled 50KN material testing machine (MTS – INSTRON Model 1341), which can provide various types of displacement inputs like, rate dependant and sinusoidal waves. The MR damper is connected to the test machine as shown in Fig. 9. The experiments are conducted by stroke-controlled mode and inputs are given through the controller.

Sinusoidal inputs for different frequencies and amplitudes are applied through the computer connected to the controller. The input signals are monitored by the LVDT and are displayed in the computer. The force time histories measured by load-cell are recorded in the data acquisition

Fig. 9 Pictorial view of experimental setup

computer. The regulated power supply source is used for different currents in the magnetic coil of the MR damper.

6. Results and discussion

6.1. Comparison of numerical simulation

Based on the numerical model as described in the Eq. (11), the numerical results are generated. The typical values of the parameters in the above equation are C_d = 18 KN-sec/m, $F_{\text{dy min}}$ = 0.6 KN, $F_{\text{dy max}}$ = 28 KN and $i_{\max}$ = 2.5A as given in Occhiuzzi, *et al.* (2003). The numerical force-displacement loops shown in Fig. 10 refers to sinusoidal displacement of 20 mm as amplitude of vibration with vibration frequency as 2.4 Hz and correspond to three different levels of current inside the damper, namely, 0, 1.5 and 2.5A. The peak damping forces are 6.02, 22.46 and 33.43 KN for 0, 1.5 and 2.5A current respectively inside the damper. The nature of force-displacement curves match well with that of Occhiuzzi, *et al.* (2003) and the peak damping forces are 6.26, 20.41 and 31.54 KN (approx.) respectively. This shows a close match with that of literature results.

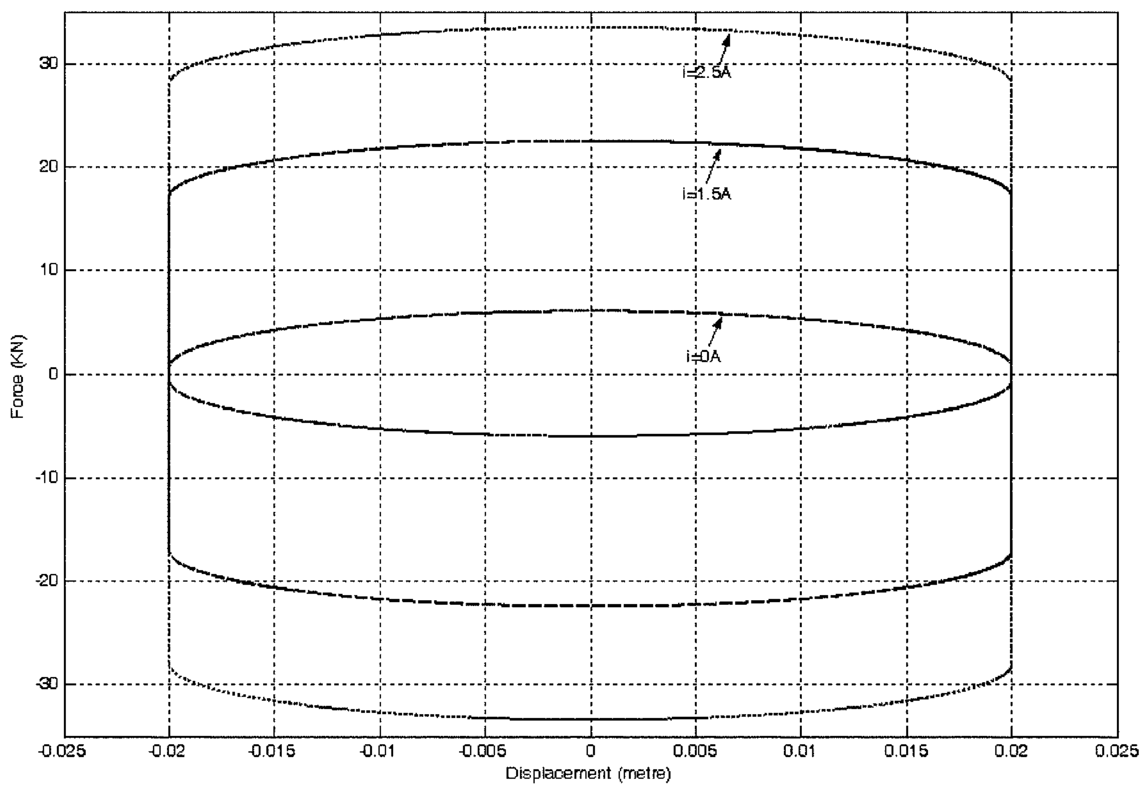

Fig. 10 Damping force vs displacement (hysteresis) with different (0, 1.5 & 2.5A) input current

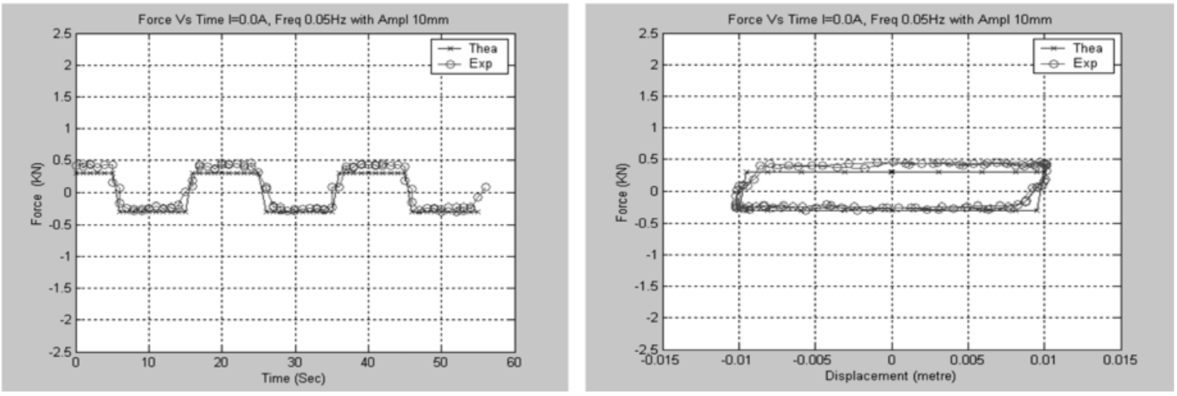

Fig. 11 Force vs time and force vs displacement graph for input current 0A frequency of 0.05 Hz and Amplitude of 10 mm

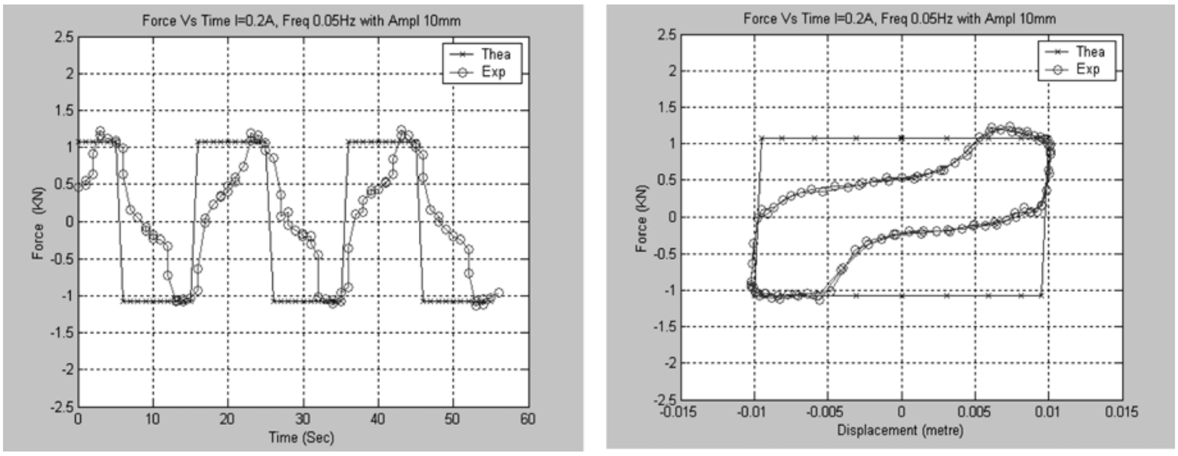

Fig. 12 Force vs time and force vs displacement graph for input current 0.2A frequency of 0.05 Hz and Amplitude of 10 mm

6.2. Comparison of numerical and experimental results

In this section, experimental results are compared with the theoretical ones. The servo-hydraulic system has some limitation in terms of displacement and frequency. The numerical results are simulated based on the possible experimental condition. The theoretical values of the parameters are $C_d = 1.143$ KN-sec/m, $F_{dy,min} = 0.6$ KN, $F_{dy,max} = 4.177$ KN and $i_{max} = 1$A for the designed damper. A sinusoidal excitation of the frequency 0.05Hz and amplitude of 10mm with variable input current of 0.0A, 0.2A, 0.3A and 0.4A is considered to present the results. The force vs time and force vs displacement are compared with the experimental results as shown in Figs. 11, 12, 13 and 14. It is observed that the simulation results match well with that of experimental one for zero current condition. Whereas, the correlation of the analysis with experiments is not satisfactory when current is applied although the trends are promising. These discrepancies may be attributed to (i) the free play between the connecting pin with the fixture and the moving jaws of the testing machine, (ii) creation of the vacuum inside the damper due to slight leakage

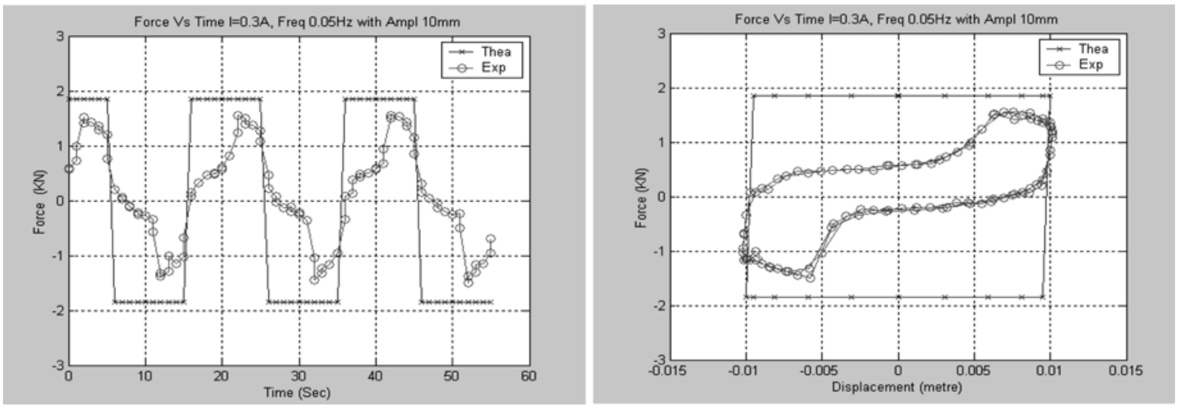

Fig. 13 Force vs time and force vs displacement graph for input current 0.3A frequency of 0.05 Hz and Amplitude of 10 mm

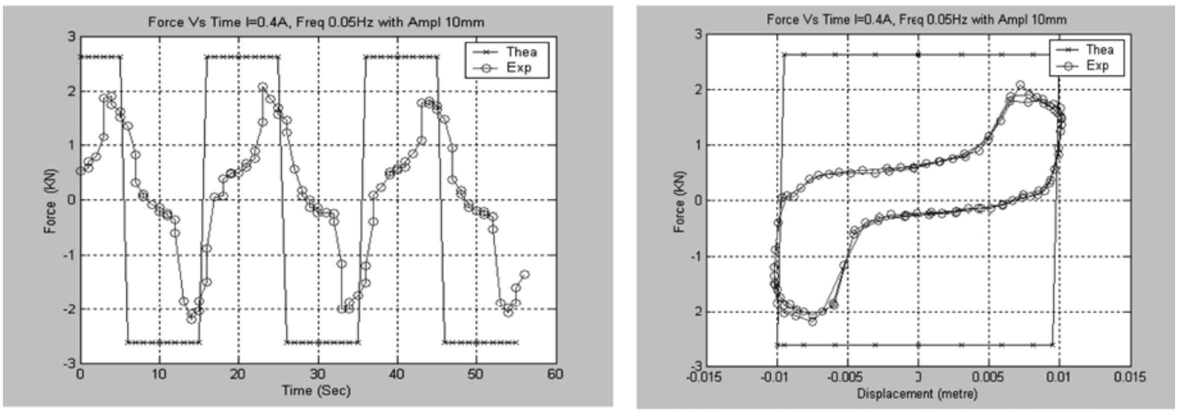

Fig. 14 Force vs time and force vs displacement graph for input current 0.4A frequency of 0.05 Hz and Amplitude of 10 mm

through the wire, and (iii) magnetic saturation of the outer cylinder and piston rod, which are path for the magnetic circuit. The experimental results are not available for higher currents due to magnetic saturation of the outer cylinder. This problem can be avoided by careful selection of high carbon steel for fabrication.

6.3. Parametric study of designed damper (Numerical)

6.3.1. Effect of current

The force vs. displacement and force vs. velocity graphs have been generated for an excitation frequency of 1 Hz and displacement amplitude of 30 mm varying the current from 0 to 1.0A in steps of 0.2A. Fig. 15(a) shows the force–displacement loop, from which it is observed that the damping force increases with the increase in the current. Fig. 15(b) shows the force–velocity loops and the graphs clearly depict the increase in force with the current as expected. The force-velocity curve as shown in Fig. 15(b) is bilinear in nature. This behaviour is expected as the MR fluid is plastic in nature both in

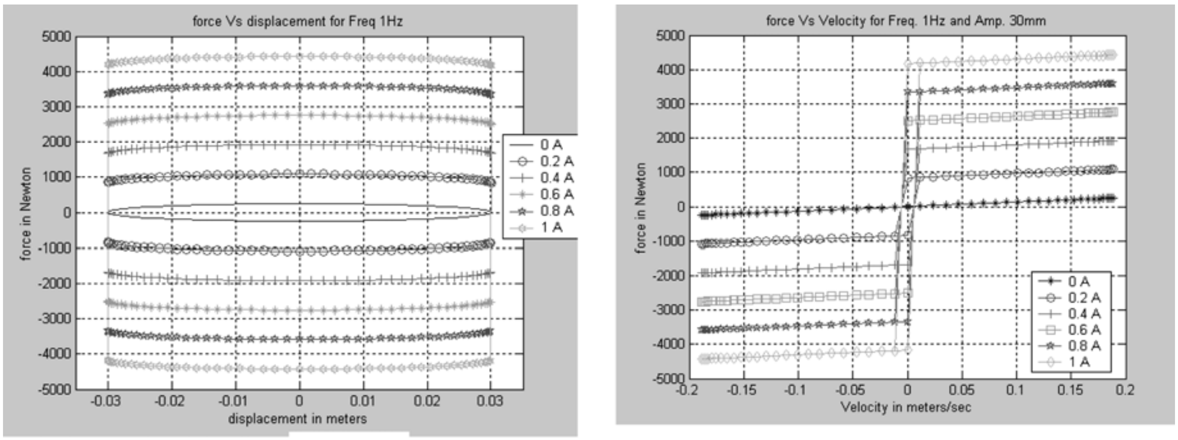

(a) (b)

Fig. 15 Force vs displacement and force vs velocity curves for a frequency of 1 Hz and amplitude of 30 mm

pre-yield and post-yield conditions. The first slope is because of the pre-yield and second slope is because of the post-yield condition.

6.3.2. Effect of amplitude

To study the effect of amplitude, force-time and force-displacement curves as shown in Figs. 16(a) and (b) have been generated for different amplitudes viz. 30 mm, 20 mm and 10 mm keeping the current constant at 0.8A and frequency of excitation at 1 Hz. From the force-displacement curves, it is observed that the maximum damping force does not change significantly, whereas the area under the curve will increase with the increase of amplitude.

6.3.3. Effect of frequency

To examine the effect of frequency, force-time plots have been generated as shown in Fig. 17 for different

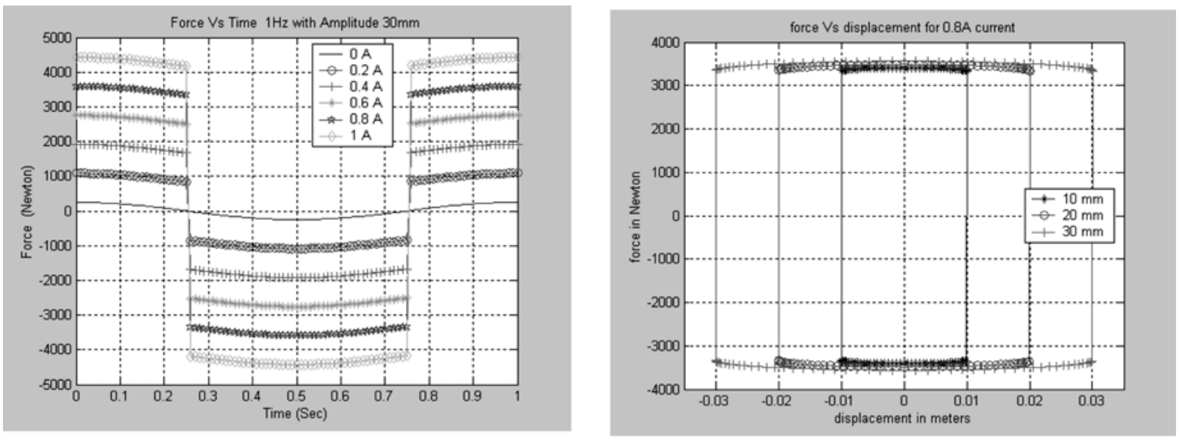

(a) (b)

Fig. 16 Force vs time anf force vs displacement curves for a current of 0.8 A and frequency of 1 Hz

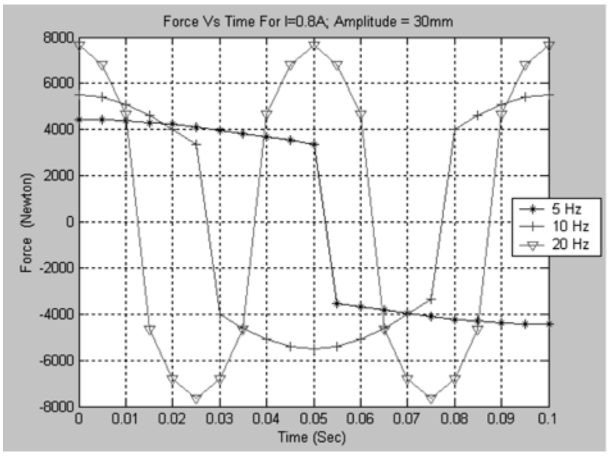

Fig. 17 Force vs. time for different frequencies

frequencies (i.e. 5 Hz, 10 Hz and 20 Hz) with fixed amplitude of 30 mm and a constant current of 0.8A. The force vs. time history curves exhibit finer elliptical peaks at higher frequencies of excitation. This may be attributed to the fact that the viscous effect is predominant compared to that of Coulomb effect.

6.4. Energy dissipation and damping coefficient

The energy dissipated by a damper over one vibration cycle is a measure of its damping capacity. The area enclosed within the force vs displacement hysteresis cycle, which is given by the integral,

$$U = \oint F dx = \int_0^{\frac{2\pi}{\Omega}} F v_p dt \qquad (12)$$

Where, Ω is the excitation frequency and v_p is damper shaft velocity. Using the experimental data and integrating it numerically, the dissipated energies are calculated for different electric field strengths and displacement amplitudes. In order to measure the efficiency of a controllable fluid damper, it is important to know the amount of damping achieved for a unit volume of active fluid. Thus for comparison purposes, it is more meaningful to calculate the dissipated energy for different current levels. In order to compare the damping performance of an MR damper with current, damping coefficients are determined by equating the energy dissipation.

$$C = \frac{U}{\pi \Omega X_0^2} \qquad (13)$$

where U is the dissipated energy and X_0 is the displacement amplitude. The damping coefficient C for amplitudes ±5 mm and ±10 mm for different currents are calculated and plotted as shown in Fig. 18.

6.5. Finite element analysis of a typical nose landing gear

A finite element model of a nose landing gear (NLG) is shown in Fig. 19. The model is developed in

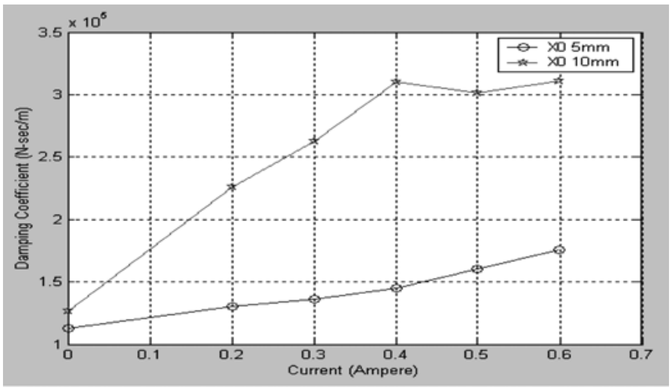

Fig. 18 Variation of damping coefficient C with input current for amplitude of 5 mm and 10 mm

MSC.NASTRAN using the pre/post processor of MSC.NASTRAN. The NLG attachments to the fuselage are simulated as pin joints by fixing the translational degrees of freedom in the FE model. The fuselage is assumed to be rigid. The finite element model is developed based on the idealization using

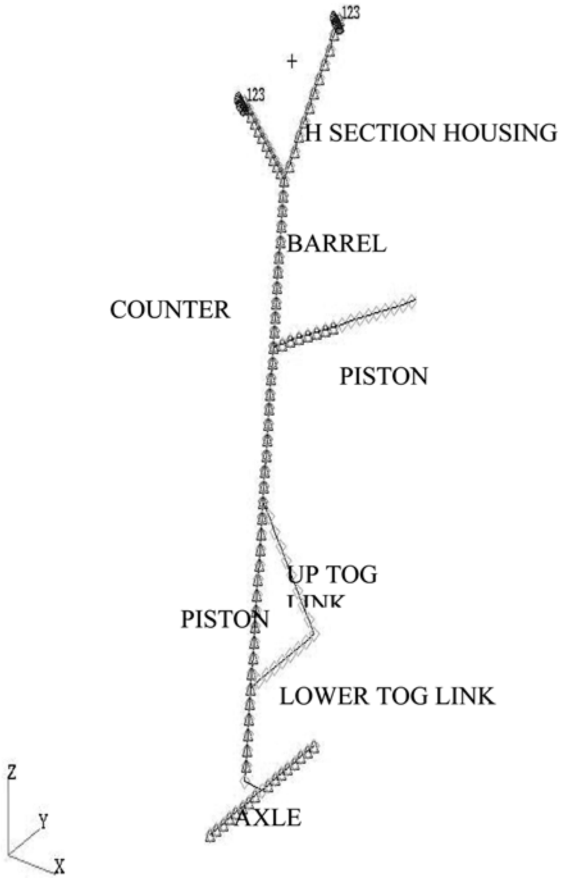

Fig. 19 FE Model of a landing gear

Table 1 Natural frequencies and mode shapes of the NLG

Mode Number	Frequency (Hz)	Description
1	21.76	Lateral bending of NLG
2	31.10	Longitudinal bending of NLG
3	67.34	Torsion rotation about vertical axis
4	93.02	Second lateral bending of NLG
5	167.87	Second longitudinal and axle bending mode

beam elements with appropriate geometric properties. The important members of the Nose Landing Gear assembly, fork, barrel (housing), inner piston, piston, upper and lower toggle links, jack-piston, wheel axle, the link to the piston and the wheel axle, are simulated in the FE model with appropriate geometric properties. The normal mode analysis is performed to determine the natural frequency and their mode shapes. The frequencies and mode shapes of first five modes of the NLG are given in Table 1.

6.6. Response analysis of NLG without MR-damper

A response model of a nose landing gear is developed based on the above modal information. A nose landing gear shares some percentage of total aircraft weight. In the present case, it is assumed that the nose landing gear will share 10% of the total aircraft weight. The load will be acting vertically through the tires. There will be ground frictional (i.e. friction coefficient = 0.3) force acting horizontally during taxing of the aircraft. The analysis is first carried out using the present numerical model developed in MATLAB and in MSC.NASTRAN with only ground friction acting for 300 msec for the comparison purpose. The assumption in this case is that two tires carry equal load. The normalized (with respect to maximum displacement) response results are shown in Figs. 20 and 21. The present simulation model shows a good match compared to that of MSC.NASTRAN.

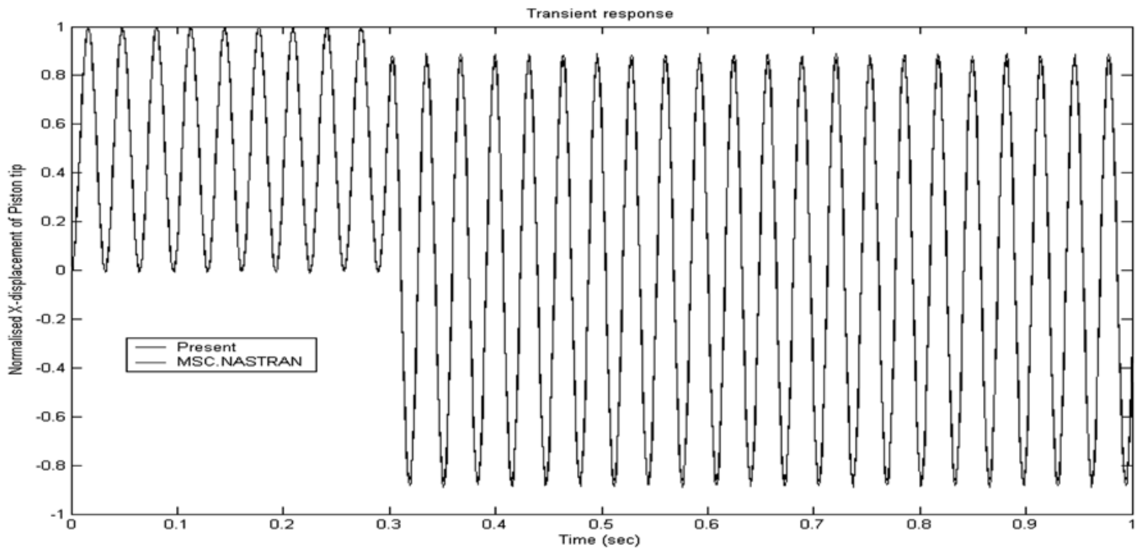

Fig. 20 Response of piston tip in x-direction due to frictional force

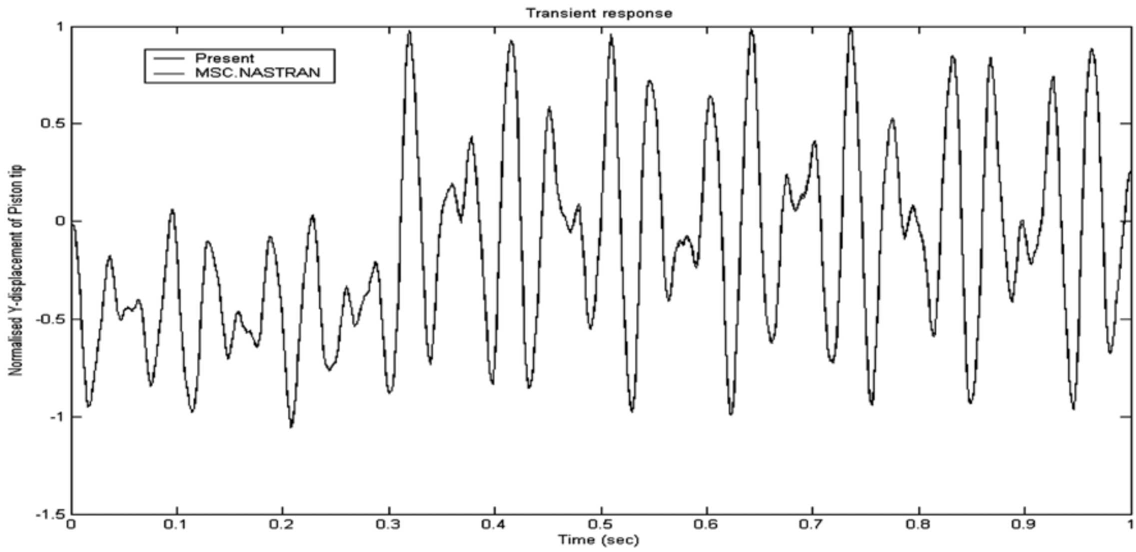

Fig. 21 Response of piston tip in y-direction due to frictional load

6.7. Open loop response analysis of NLG without and with MR-damper

The response analysis is carried out with actual loading conditions (i.e., vertical self weight of aircraft and horizontal frictional load acting for the whole duration). Initially the analysis is carried out

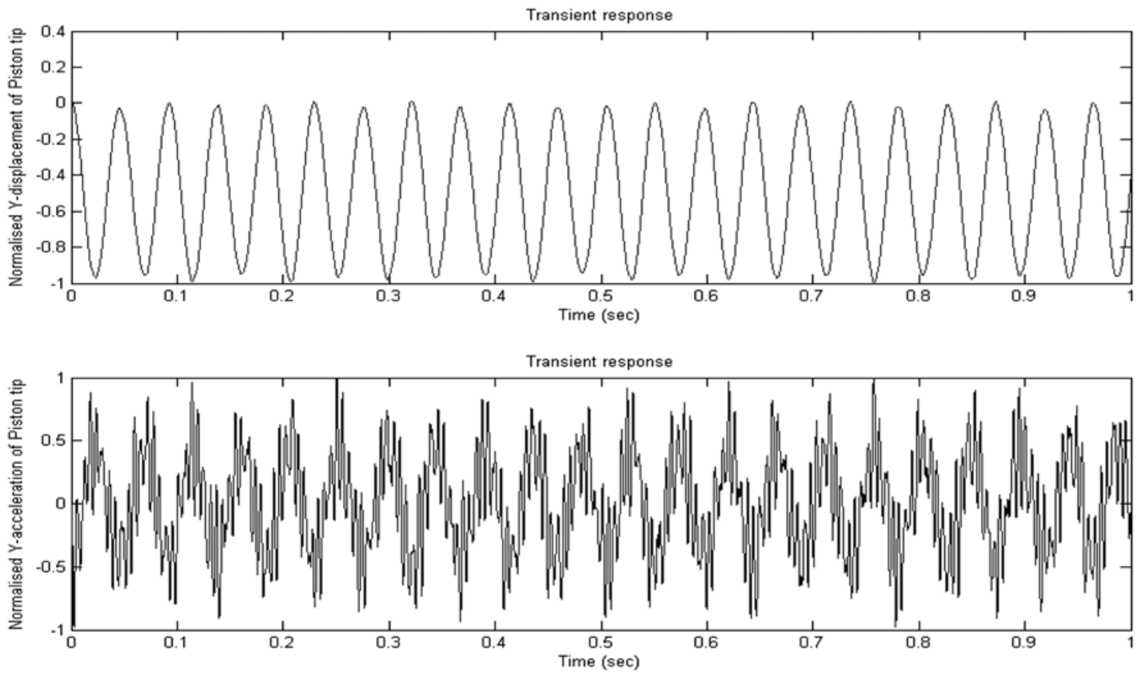

Fig. 22 Response of piston tip in y-direction due to vertical and frictional loads

Table 2 Summary of response results at piston tip with balanced loading case

Applied current (A)	Equivalent damping coefficient (c_d), N-s/mm (Amplitude 1 mm)	RMS acceleration, g
Without damper	-	0.5903
0.0	1.1196	0.3766
0.2	2.1849	0.3714
0.4	3.2501	0.3685
0.6	4.3153	0.3662
0.8	5.3806	0.3640

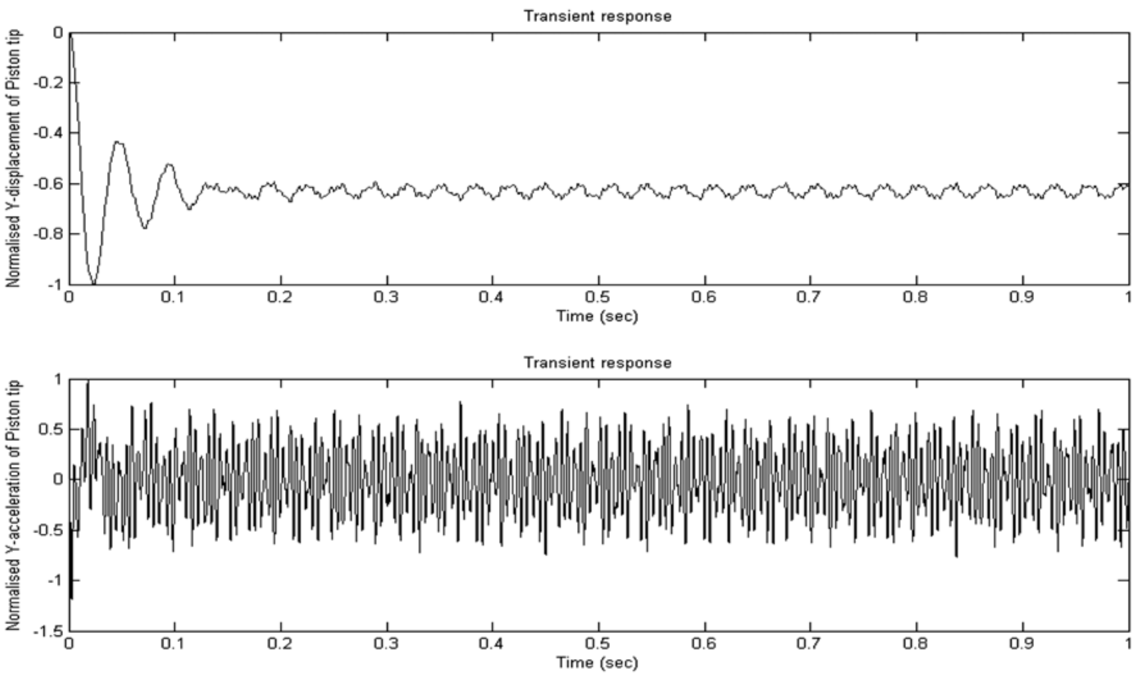

Fig. 23 Response of piston tip in y-direction due to vertical and frictional loads with MR-damper

considering equal share of loads by two tires. The lateral (y-direction) deflection and acceleration responses at piston tip are shown in Fig. 22. The RMS acceleration at piston tip in lateral direction is 0.5903 g. The acceleration level can be reduced implementing a MR-damper in the system. The results are generated with a MR-damper in the system and varying the current though the coil. The lateral response of the piston is shown in Fig. 23 with MR-damper as semi-active device. The results summary is shown in Table 2. It is observed that there is a significant improvement in the system performance. But it is limited to monotonic improvement in the system performance with increase in current through the coil. This may be due to saturation in the system performance. The above loading condition is an ideal one. In reality, the loading may not be perfectly balanced. The second loading case is considered as an imbalance in tire loading. It is assumed that the left and right tires share loads in a proportion of 40% and 60%, respectively. The results are generated for the above loading conditions and ground

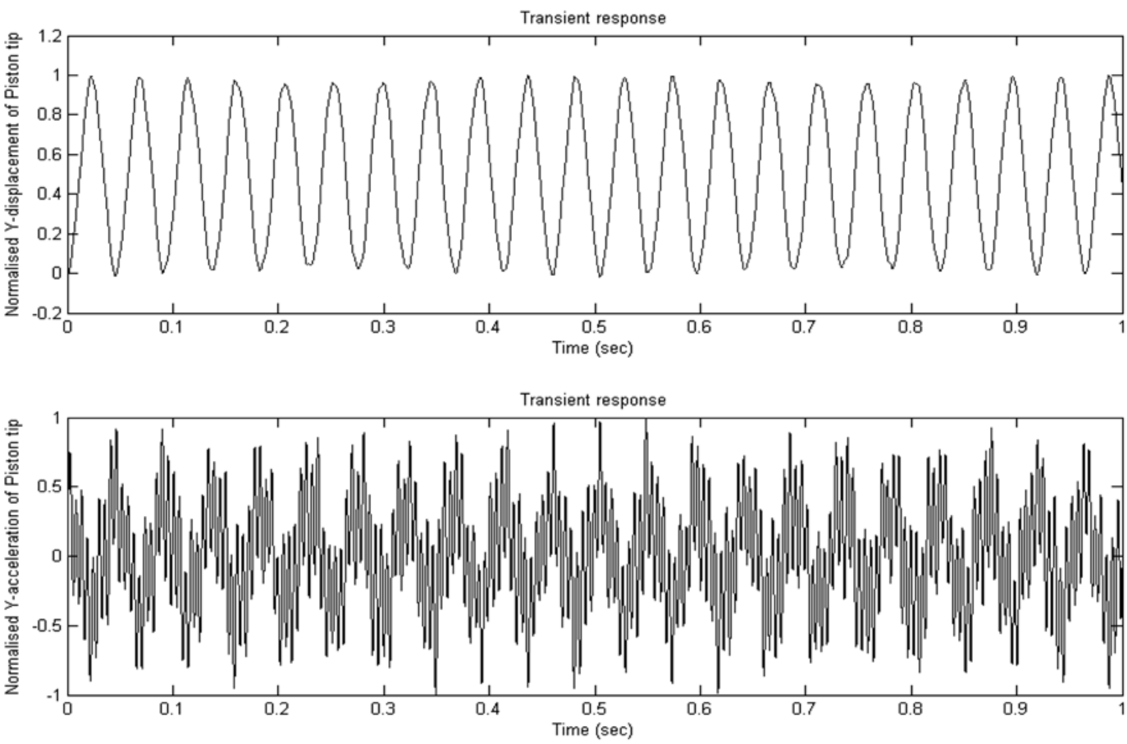

Fig. 24 Response of piston tip in y-direction due to vertical and frictional loads

Table 3 Summary of response results at piston tip with imbalanced loading case

Applied current (A)	Equivalent damping coefficient (c_d), N-s/mm (Amplitude 1 mm)	RMS acceleration, g
Without damper	-	3.3881
0.0	1.1196	1.2112
0.2	2.1849	0.9306
0.4	3.2501	0.8071
0.6	4.3153	0.7341
0.8	5.3806	0.6842

frictional force and shown in Fig. 24. The RMS acceleration in lateral direction is 3.3881g. The acceleration level is high compared to that of balanced loading. This indicates the source of vibration in a nose landing gear of an aircraft. In this case also the effect of MR-damper is studied and summary of results are presented in Table 3. The numerical results reveal that MR-damper is a good semi-active candidate for vibration reduction in a dynamic system.

7. Conclusions

In this paper, the fundamental behaviour of MagnetoRheological (MR) damper has been modelled for analysis and design of orifice flow damper. The designed damper has been fabricated and tested.

Analytical and experimental results have shown that the present method of analysis and design of MR damper is capable of capturing the characteristics of double-ended flow damper.

The mathematical model of a typical nose landing gear is also developed to study the vibration characteristics due to ground excitation. The numerical results are validated for open loop analysis. The response levels are monitored at the piston tip for various loading conditions. The second loading condition indicates the source of vibration in a nose landing gear of an aircraft. The response levels are also monitored with MR-damper as semi-active device. The numerical study reveals that MR-damper is a good candidate for vibration reduction in aircraft nose landing gear system.

Acknowledgements

The authors are grateful for the support given by Aeronautical Development Agency, Bangalore to carry out the research work. The authors are thankful for MR-fluid and the experimental facility provided by ACD and SID of NAL, Bangalore, respectively.

References

David, Carlson J. (2001), "What makes a good MR fluid?", *Proceeding of 8th International Conference on ER Fluids and MR Fluids Suspensions*, Nice, July 9-13.

Dyke, S. J., Spencer, B. F., Sain, M. K. and Carlson, J. D. (1996), "Seismic response reduction using magnetorheological dampers", *Proceeding of the IFCA World Congress*, San Francisco, California, June 30-July 5.

Gavin, Henri, Hoagg, Jesse and Dobossy, Mark (2001), "Optimal design of MR dampers", *Proc. of U.S.–Japa workshop on Smart Structures for improved Seismic Performance in Urban Regions,* Seattle WA, 225-236.

Gravatt, John W. (2003), "Magneto-rhelolgical dampers for super – sport motorcycle applications", MS Thesis, Department of Mechanical Engineering, Virginia Polytechnic Institute and State University.

Jolly, Mark, Jonathan, R., Bender, W. and Carlson, J. David (1998), "Properties and application of commercial magnetorheological fluids", *Proceeding of SPIE on Smart Structures and Materials*, San Diego, 3327, 262-275.

Kang, Hao (2001), "Rotor blade lag damping using embedded chordwise absorbers", Ph.D. Dissertation, Department of Aerospace Engineering, Pennsylvania State University, August.

Kelso, Shawn P. (2001), "Experimental characterisation of commercially practical magnetorheological fluid damper technology", *Proceedings of SPIE Conference on Smart Structures and Materials*, Newport Beach, CA, March.

Kruger, Wolf (2000), "Integrated design process for the development of semi-active landing gears for transport aircraft", Ph.D. Dissertation, University of Stuttgart, Germany.

Lord Materials Division (1999), "Designing with MR fluids", Lord Corporation Engineering Note, December.

Lord Materials Division, "MagnetoRehological Fluids", Lord Corporation Engineering Note, http://www/lord.com.mr.

Occhiuzzi, A., Spizzuoco, M. and Serino, G. (2003), "Experimental analysis of magnetorheological dampers for structural control", *Smart Mater. Struct*., **12**, 703-711.

Simon, David E. (1998), "Experimental evaluation of semiactive magnetorheological primary suspensions of heavy truck", MS Thesis, Mechanical Engineering, Virginia Polytechnic Institute and State University.

CC